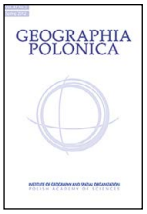

Geographia Polonica
2025, Volume 98, Issue 2, pp. 121-147
https://doi.org/10.7163/GPol.0296

INSTITUTE OF GEOGRAPHY AND SPATIAL ORGANIZATION
POLISH ACADEMY OF SCIENCES
www.igipz.pan.pl

www.geographiapolonica.pl

SEA LEVEL RISE EFFECT ON INHABITED RIVER-DELTAIC ESTUARINE ISLANDS IN THE TROPICAL MONSOON REGIONS IN THE INDIAN SUNDARBANS

Rituparna Acharyya[1] • Niloy Pramanick[2] • Rishin Basu Roy[3] • Masuma Begum[4] • Arjan Basu Roy[5] • Devsena Roychaudhury[5] • Anasua Pal[5] • Anushka Chakraborty[5] • Prasun Majumder[5]

[1] Faculty of Geographical Sciences
Kazimierz Wielki University
Plac Koscieleckich 8, 85-064 Bydgoszcz: Poland
e-mail: rituparna.acharyya@ukw.edu.pl (corresponding author)

[2] School of Oceanographic Studies
Jadavpur University
Kolkata, West Bengal: India

[3] Department of Environmental Science
University of Calcutta
Kolkata, West Bengal: India

[4] Directorate of Forests
Government of West Bengal
Kolkata, West Bengal: India

[5] Nature Mates-Nature Club
Kolkata, West Bengal: India

Abstract

Coastal deltaic landscapes under tropical monsoon regions are sensitive to sea level changes exacerbated by human interventions. In low-lying areas, rising relative sea level (RSL) and such interventions are intensifying geohazards like coastal erosion and land subsidence. This study examines erosion and flooding risks in the Sundarbans mangroves along the Bay of Bengal using statistical models – Endpoint Rate (EPR) and Shoreline Change Envelope (SCE) incorporated in Digital Shoreline Analysis System (DSAS). "Patharpratima Block" comprises thirteen estuarine islands, part of the delta formed via confluence of three rivers, the Ganges, the Brahmaputra, and the Meghna. EPR and SCE were applied via geospatial modelling, and remote sensing to evaluate coastal changes between 1990-2020. Results show the shoreline undergoes gradual to significant changes due to fluctuating erosion and deposition, impacting local residents. Surendranagar and Dhanchi were identified as the most vulnerable, followed by moderately vulnerable Lothian. With observed RSL rise, shoreline dynamics were modeled using EPR and SCE to estimate past and future changes. Additionally, the Sundarban Reserve Forest (SRF), the world's largest mangrove forest, is at risk of disappearing. The region's population has increased, while total area has shrunk due to erosion. Urgent sustainable measures are needed to prevent biodiversity loss and displacement of livelihoods into environmental refugees.

Keywords

sea level rise • river estuarine islands • shoreline • coastline • geospatial modeling • Patharpratima Block

Introduction

Coastal erosion refers to the removal and redistribution of solid materials from the coastline due to erosion and deflation caused by coastal and tidal currents. (Prasad & Kumar, 2014; Central Water Commission, 2016). Coastal erosion process involves withdrawal of materials from the coast due to supply imbalances and abrasion at the foreshore (Marchand, 2010). According to the National Geographic Society (2020), coastal erosion occurs from the gradual wearing down of rocks along the shore due to waves and currents. Short-term damage can result from turbulent waves and currents without significant coastal improvement. Coastal erosion is commonly measured in cubic meters per meter per year ($m^3 \cdot m^{-1} \cdot year^{-1}$) or meters per year ($m \cdot year^{-1}$) for coastal degradation. It affects over 80% of the world's coastlines, with erosion rates ranging from 1 $cm \cdot year^{-1}$ to 30 $m \cdot year^{-1}$ (Mangor et al., 2017; Nath et al., 2022). Since the coastal environment is diverse and constantly changing, it is more difficult to determine the extent of erosion. Thus, several factors affect coastal erosion, such as increasing sea levels, wind, tide, waves, storm surges, etc. Destructive waves are primarily known for crashing off the landmass to induce degradation along the coast (Geological Survey Ireland, 2020). While heading to the shore, waves bear enormous energy dissipated by breaking waves, generating tides, shifting water temperature, swirling sediments, turbulence, and heat (Mohr, 2001). When waves break and recede across the coast, they create longshore movement and accumulate sand (National Ocean Service, 2020). The coastal area is also affected by changing weather conditions such as wind, currents, and tides (Smithsonian, 2020). There are various kinds of temporal and spatial patterns of coastal degradation (Cai et al., 2009; Farquharson et al., 2018), can be categorized temporally, e.g., prolonged erosion due to Sea-Level Rise (SLR), river system disruption, or decreased sediment flux (FitzGerald et al., 2008; Cai et al., 2009). Rising sea levels could inundate terrestrial habitats and affect estuarine and coastal freshwater systems through increased tidal intrusions and salinity levels. Consequently, coastal erosion is anticipated, leading to the landward displacement of coastal habitats and the redistribution of shallow intertidal and marine habitats (Paice & Chambers, 2016).

"Shoreline" and "coastline" are often used interchangeably, but they have distinct meanings. "Coastline" refers to the sea-facing boundary including land and water features, while "shoreline" specifically denotes the line connecting land and water (Mohan, 2005) The complex land/water boundary line connecting contact points between land and water bodies is called the shoreline (Nandi et al., 2016; Roberts, 2019). The coastline marks the boundary where an island or continent ends, known as the continental plate's margin (Roberts, 2019). The shoreline position changes due to factors such as river flow, rising sea levels, geomorphologic alterations, and seismic shifts (Scott, 2005). When materials are removed from the shoreline faster than they are replenished, it causes shoreline erosion, leading to the landward movement of the shoreline (Central Water Commission, 2016). One of the primary causes of shoreline erosion is wave action (Nehra, 2016), which determines the shape and structure of the shore. Wave action controls the movement of sediment from estuarine and marine areas to the shoreline through accretion (Inman et al., 2005). When waves hit the shoreline at an angle, they create a longshore current. The tidal wave causes lower beach degradation in the subtidal environment while the upper level remains exposed with a specific structure (Cai et al., 2009). Beaches are composed of varying-sized sediments, from large rocks to fine sand or mud, which are moved by wave action (Columbia University, 2020). Rising sea levels unequivocally impact weaker coasts the most, leading to coastline retreat (Committee on Climate Change, 2010).

The dynamics of sea, wind, waves, and environmental changes can be intensified via anthropogenic disruptions are among the

main causes of erosion (Yincan et al., 2017). Anthropogenic activities often contribute to coastline and shoreline changes (Nandi et al., 2016). Coastal regions are highly vulnerable to human-caused disruptions such as population growth, urbanization, tourism, dam construction, industrialization, and pollution (Sondi et al., 2008). Coastal areas with high populations face various hazards like erosion, flooding, and coral bleaching (Prasad & Kumar, 2014). Due to excessive sand mining, waves permanently alter the shape and structure of coastlines and shorelines as sand loosens and moves out rapidly (Prasad & Kumar, 2014). In addition to sand mining anthropogenic activities like seabed dredging and constructing coastal structures can trigger profound alterations to the shoreline (Thakur et al., 2021). In coastal areas, floodplains, deltas, estuaries, and wetlands are forming "River Deltaic Estuaries" (RDEs), which are sensitive to aforementioned anthropogenic operations and consequent climate change (Li et al., 2011). RDEs are sediment accumulation zones that are at risk of coastal erosion due to decreased water flow and the presence of wetlands (Masselink & Russell, 2013; Acharyya et al., 2023). Massive sediment outflows from the estuarine reaches, and resultant coastal erosion is affecting estuaries worldwide (Ghosh et al., 2014). Around 61% of the world's population lives along coastal margins; since RDEs are also heavily inhabited, intensifying anthropogenic activities render them vulnerable to coastline and shoreline erosion (Alongi, 1998). The runoff and sediment out-flux from the watershed can cause significant erosion and changes to nearby shorelines and coastlines (Acharyya et al., 2023)

While a certain level of natural continuity can be preserved in the coastal environment; however increased human modification decreases "naturalness" (Prasad & Kumar, 2014). With the increased release into the atmosphere of carbon dioxide (CO2) and other greenhouse gases, global warming is estimated to accelerate by about 3°C by 2030 (McSweeny, 2020). Over the upcoming few years, this increase will increase global sea levels by up to 5 meters, which is a brief period for the occupation of the coast by humans (Oliver-Smith, 2009). Sustainable coastal planning and engineering strategies provide information about the shoreline's current, historical, and projected positions in long-term. In coastal protection, this information is essential for validating models, assessing SLR, and identifying hazard zones (Oppenheimer et al., 2019). GIS and Remote Sensing have contributed significantly to shoreline change analysis and monitoring (Kundu et al., 2014). Remote sensing supports conservation survey findings with cost-effective and precise information, as satellite imagery analysis demonstrates the effectiveness of studying coastal processes. Future projections of shorelines are necessary for planning purposes since they provide insight into the rate at which the region is changing (Kundu et al., 2014). Precise and integrated information on past and present shoreline positions is essential for potential shoreline predictions (Nandi et al., 2016). Different models can be used to predict shorelines in a GIS-based environment. These include the End Point Rate (EPR) model, Shoreline Change Envelope (SCE), Jackknife model (JK), Linear Regression model (LR), and Average of Rates (AOR). These models can be evaluated using historical data, enabling assessment of erosion and accretion scenarios for shorelines along water bodies (Maiti & Bhattacharya, 2009; Mukhopadhyay et al., 2012). The EPR model forecasts future shoreline positions based on chronological change rate data, while the LR model uses robust linear prediction for short-term adjustments and long-term shoreline data (Nandi et al., 2016). Several researchers used the EPR model to forecast shoreline changes (Adarsa et al., 2012; Mukhopadhyay et al., 2012). Adarsa et al. (2012) have estimated the rate of transition in the shoreline position of estuarine Ghoramara Island using the methods of EPR, LR, NSM and cross-validation regression coefficient. Both Kundu et al. (2014), and Nandi et al. (2016) have employed application of DSAS

part of the "Coastal Transition Hazards" by USGS (Himmelstoss et al., 2018) to cast a transect (*xn*) and calculate the changes using the NSM method. The SCE provides values in precise distance measurements rather than rates like EPR. SCE calculates the distance between shorelines along the transect, generating only positive values since distance is inherently non-directional (Kundu & Mandal, 2024). For this investigation, EPR and SCE were selected as the most effective statistical techniques for analyzing coastline and shoreline dynamics. Previous studies (Acharyya et al., 2023; Pramanick et al., 2022) have demonstrated that both methods effectively assess coastal changes over time while requiring minimal input data.

The parameter of sea surface temperature (SST) considered in this study is mainly attributed to its increase, due to the increase in tropical cyclones encountered over the Bay of Bengal over the last decade (Ghosh et al., 2001; Hazra et al., 2016). SST data obtained at various depths using various equipment, including satellite infrared and microwave radiometers, as well as anchored and floating buoys and boats (Remote Sensing Systems, 2020). The change in annual mean SST over the Bay of Bengal from 1990 to 1998 was analyzed by Hazra et al., (2016) using "NOAA AVHRR" data and was approximately 0.8°C higher in 1998 than in 1990. Due to observed climate changes, specifically warming associated with increased sea surface temperatures (SST), there has been an increase in sea level in the Bay of Bengal. This increase was documented from 1993 to 2000 and has been assessed to estimate sea surface height (SSH) using satellite altimeter data from the TOPEX/POSEIDON mission (Ghosh et al., 2018). SSH is also considered here and analyzed using an estimate called Relative Sea Level (RSL). RSL refers to the observed sea level in comparison to a land-based reference frame or SSH, incorporating dynamic inputs from ocean circulation and changes in the geoid relative to the corresponding ellipsoid (European Space Agency, 2020).

This study assesses the coastal change of the estuarine Patharpratima Block in West Bengal's Sundarban mangroves by considering the shoreline and coastlines from 1990-2020 and evaluating the future scenario. Multispectral satellite data from Landsat (TM and OLI) between 1990-2020 has been used to delineate coastlines and shorelines during the same period and to assess the spatiotemporal change by incorporating the statistical models EPR and SCE incorporated into DSAS and to predict a future scenario based on those models. Also, the evaluation considers the influence of SST, SSH, rainfall, atmospheric temperature, vegetation, and population on the spatiotemporal coastal dynamics in the study area.

Study area

The study area, Patharpratima CD (Community Development) Block in the Indian State of West Bengal (88°38'-88°30' East; 21°38'-22°02' North) covers an area of 484.47 km^2 and is part of the Ganges-Brahmaputra-Meghna (GBM) Delta, bordered on the East by Bangladesh, west by the Hooghly River, south by the Bay of Bengal (Dhara & Paul, 2016; Mandal et al., 2022). Administratively it is part of the Kakdwip sub-division under the South 24 Parganas district, bordered by the CD Block of Namkhana, Kakdwip, Mathurapur, and Kulpi (Dhara & Paul, 2016). As per the 2011 census, Parthapratima Block had a population of 328,769 with a density of 678 people/km^2 (Dhara & Paul, 2016). The predominantly rural area includes 92 inhabited villages, 33 on the mainland, and the rest on a group of 13 coastal-estuarine islands (Mandal, 2021).

The study area (Fig. 1) includes the mainland, Dakshin Gobindapur, and coastal-estuarine islands, such as Lothian, Dhanchi, Surendranagar, Patharpratima, Chotarakhsashali, Rakhalpur, Shibnagar, Paschim Sripatinagar, Bhagabatpur, and Maheshpur. These islands are part of the RDE system of the Indian Sundarban mangroves, located in the lower part of the GBM Delta, formed

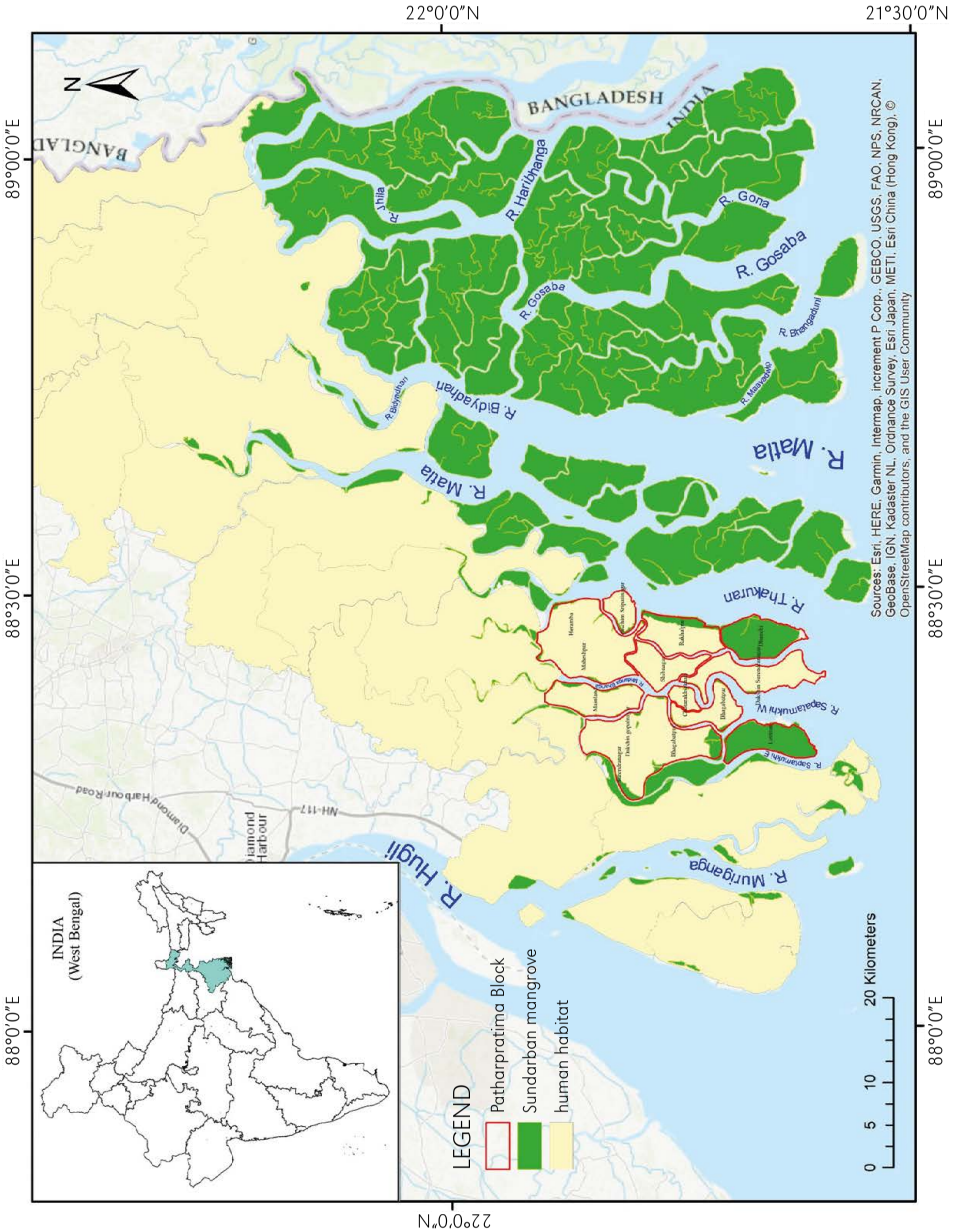

Figure 1. Location map of the study area

by the confluence of the rivers flowing into the Bay of Bengal (Dhara & Paul, 2016; Mandal, 2021; Rukhsana & Hasnine, 2024). To be more specific, the study area lies within the Hugli-Saptamukhi River-Dominated Estuary (RDE) complex of the Sundarbans estuarine system (Mandal et al., 2022), one of the most dynamic ecological and geomorphological regions of the lower Ganges-Brahmaputra-Meghna (GBM) delta plain, situated at an elevation of approximately 4 meters above Mean Sea Level (MSL) (Dhara, 2019). Additionally, coastal islands in low-lying regions, such as the GBM delta, are especially vulnerable to flooding, storm surges, and severe cyclones (Brown & Nicholls, 2015). As per various studies, climate change has led to more frequent and intense extreme weather events and shifts in temperature and precipitation patterns (Dube et al., 2006; Ghosh et al., 2014; Hazra & Samanta, 2016; Mukherjee & Siddique, 2018). Patharpratima, has undergone substantial land reclamation due to the development of rural settlements, aquaculture, and agricultural expansion causing removal of natural vegetation, particularly mangroves, as physical barriers against cyclonic disruptions (Sreelekshmi et al., 2023). The study area faced major setbacks due to highly severe tropical cyclonic events such as Sidr Cyclone (November 2007), Aila (May 2009), Bulbul (November 2019), Amphan (May 2020), and Yaas (May 2021), occurring 6–12 months before landfall in the recent past (Bhattacharya et al., 2014; Halder & Bandyopadhyay, 2022; Kar & Basu, 2023). These cyclonic disturbances have compromised the physical barriers provided by mangroves, which are essential for maintaining the region's shoreline dynamics (Paul et al., 2024). Cyclonic disturbances accelerate processes like overwash (the flux of sediment and water on the coast during cyclones) and coastal erosion markedly (Paul et al., 2024). Coastal land degradation and saltwater intrusion have severely impacted agriculture, fisheries, and livelihoods in the research area. This study focuses on evaluating the changes in the coastline and shoreline of the estuarine islands in the Patharpratima Block due to these issues. Sidr damaged 24.1% of the forest, resulting in $142.9 million in losses (Saadi, 2010). Aila destroyed over 500 km^2 of agricultural land in West Bengal, costing $26.3 million. Bulbul caused approximately $3.4 billion in damages and affected 3.5 million people (Basu, 2019). Cyclone Amphan impacted 283 km^2 of Sundarbans mangroves and flooded 12.3% of southern West Bengal (Das et al., 2020). Cyclone Yaas hit coastal West Bengal with winds over 120 km/h, damaging 58.74 km^2 of Pathar Pratima (Paul & Chowdhury, 2021).

Materials and methods

Data and software

In this study, the multi-temporary satellite imageries of the various resolutions Landsat TM and OLI/TIRS were employed (Tab. 1). Landsat data for coastal areas are commonly used for their multi-temporal as well as multi-spectral data capacities. According to Table 1, Landsat satellite data were collected over five years, from 1990 to 2020, to establish a coherent framework for monitoring the coastline and shoreline dynamics in the study area. The chosen dates for acquiring satellite datasets align with data availability, ensuring precision and quality critical for maintaining accuracy in the current study's analysis. In addition, data on shorter intervals between 2015 and 2020 have been selected, as this period aligns with the increased frequency of cyclonic events that affected the study area.

The study used an image processing application for optical image analysis and statistical analysis of DSAS within a GIS environment. DSAS Version 4.5 with the geospatial interface is crucial for providing detailed regression statistics in a reproducible manner applicable to large datasets (Himmelstoss et al., 2018). The DSAS statistical model with a geospatial interface uses temporal trend analysis to measure the position and geometry of past and current shorelines

and coastlines. It offers the advantage of calculating change rate statistics over a temporal series of coastline and shoreline positions in coastline change research (Oyedotun, 2014). In this study, DSAS was employed to study the transition in coastline and shoreline and all associated estimates linked to SCE and EPR models. The appropriate inputs for the tool include the vector formats of the coastline and shoreline, the date, and the transect (xn) length of the coastline and shoreline.

Table 1. Details of the Satellite datasets used for the current study

Satellite / Sensor	Path / Row	Date of Acquisition
LANDSAT 5-TM	138/45	14.01.1990
	138/45	28.01.1995
	138/45	06.01.2000
	138/45	07.01.2005
	138/45	06.02.2010
LANDSAT 8-OLI	138/45	08.03.2015
	138/45	11.01.2018
	138/45	01.01.2020

Methods

Data processing

Figure 2 shows a flow chart of all metrics used in this study's data. The study is covered by satellite imagery of Landsat 5 TM and 8 OLI/TRS provided were rectified geometrically, followed by radiometric corrections for each satellite band. It takes two steps: Digital Number (DN) data are translated into radiance values, and then the radiation values are turned into reflectance values.

Delineation

Automated shoreline and coastline delineation, a process of significant complexity, is challenged by the persistent presence of a saturated water layer between the land and water interface. This study used the Tasseled Cap Transformation technique to delineate the shoreline and coastline. To ensure precision in boundary assessment, we have implemented a range of indices, including NDVI (Normalized Difference Vegetation Index), NDWI (Normalized Difference Water Index), EVI (Enhanced Vegetation Index),

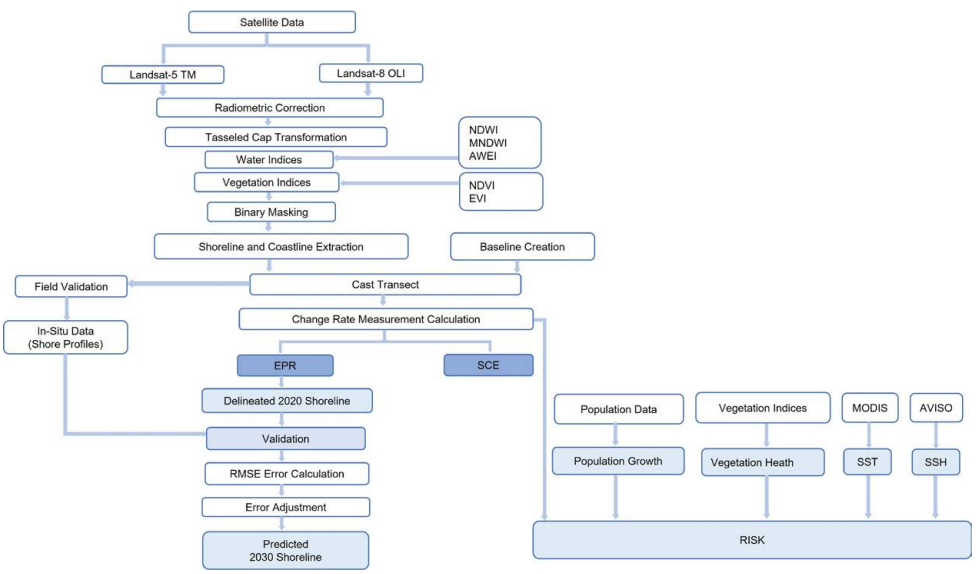

Figure 2. Flow chart showing methodology of the current study

AWEI (Automated Water Extraction Index), and MNDWI (Modified Normalized Difference Water Index). Subsequently, strips of selected imageries were extracted along the coastlines and shorelines to convert them into binary images.

Automated coastline and shoreline delineation is a dynamic process due to the presence of water-saturated zones at the land-water boundary (Maiti & Bhattacharya, 2009). Here, the technique of Tasseled Cap Transition for coastline/shoreline extraction, which has been employed by Huang et al. (2002) derived from EROS (Earth Resource Observation and Science), the coefficients for converting the Tasseled Cap Landsat data. The processed images (listed in Tab. 1) show the persistent positions of the coastline and shoreline, tracked progressively over eight periods within the 5-year intervals (1990-2020), as indicated in Table 1. The binary raster imagery is then converted into a dataset for the vector, outlining the borders of the coastlines and shorelines in the study area.

Method of casting transect from baseline

This technique is primarily based on statistics. Before constructing the transect, a solitary baseline is formed, each from the coastline and shoreline. There are two primary baseline delineation methods: buffering method and baseline creation from a certain distance (Nandi et al., 2016). The buffer technique is the most precise and accurate way to limit baselines since it takes the same sinuous form as the neighboring shoreline (Nassar et al., 2019). The DSAS software's baseline measurement includes attribute fields that provide essential information about the transect order and the baseline location for the coastline and shoreline. The baseline is calculated at a buffer distance of 1000 m offshore from the nearest coastline and shoreline of the study area. Thus, for different years under study, the transect lines have been cast orthogonally from the coastline as well as the shoreline.

Shoreline and coastline change rate assessment methods

In this study, two main statistical models, the EPR (End Point Rates) and SCE (Shore Change Envelope), have been used to calculate the change rate in the coastline and shoreline of the islands of Patharpratima Block.

The EPR is calculated by dividing the distance between the previous and current positions of coastlines/shorelines by the time interval between them. The EPR for the study region is computed using equation 1, which has also been used in earlier studies (Bheeroo et al., 2016; Pramanick et al., 2022; Acharyya et al., 2023; Hasanuzzaman et al., 2023) which is as follows:

$$S_r = f_o - f_y / n \quad (1)$$

where:

S_r = annual bank line change rates (meter·year^{-1});
f_o = distance (in meters) between the created baseline and coastlines/shorelines of the earliest date (x_n);
f_y = distance (in meters) between the current coastlines/shorelines and the earliest date's coastlines/shorelines;
n = number of years between the study's earliest date and the recent date.

SCE is usually determined as the interval between the coastlines or shorelines that are furthest and closest to the baseline (Pramanick et al., 2022; Acharyya et al., 2023). Using SCE, the positions for each transect indicate the cumulative variances in coastline/shoreline movements. Equation 2 shows the SCE, which is expressed as:

$$S_d = d_f - d_c \quad (2)$$

where:

S_d = coastline/shoreline change distance (m);
d_f = distance from the created baseline to the farthest coastlines/shorelines at a particular transect (x_n);
d_c = distance between baseline and closest coastlines/shorelines at the at a particular transect (x_n).

Then prediction assessment in DSAS is also executed using Equations (3-5)

$$S_{pn} = s_l \cdot t_i + i_{pt} \quad (3)$$

S_{pn} = shoreline/coastline position for considered time intervals (t_i).

Then Equations 4 is used to estimate the slope (s_l) by calculating the change in the position of the shoreline between the oldest shoreline position (f_o) during the earliest considered time interval (t_o) and the most recent time interval (t_y).

$$S_{pn} = \frac{f_o - f_y}{t_o - t_y} \quad (4)$$

Following the slope's derivation, the distance between the closest and furthest shoreline positions from the baseline, designated as intercept (i_t) is computed using Equation 5.

$$ipt = f_o - (s_l \cdot t_o) = f_y - (s_l \cdot t_y) \quad (5)$$

The baseline, i.e. intercept (i_{pt}), is considered constant until the future time interval denoted as Tf, based on the future location of the shoreline (f_p) is projected from the youngest shoreline position (f_y) at t_y using Equation 6, which is estimated via reformulation of Equation 4.

$$f_p = s_l \cdot t_o - t_y + i_{pt} \quad (6)$$

Calculation of net areal change

This method delineates the accretion and erosion zones and calculates the spatial changes in the Patarpratima block's islands. In GIS environment, the spatial analysis examined the islands' spatial for specific years by creating polygons along their borders to determine their areal extent. The islands' net aerial change and erosion are computed from 1990 to 2020 as a result of overlay techniques, wherein two coastlines are linked with the "union" overlay operation. Thus, the distribution of areas that underwent erosion-accretion has occurred along the shoreline and coastline is estimated using the created polygons. The vector dataset is converted into a raster dataset for aerial change calculations using a 10-meter grid size.

Estimation of sea surface height

The global dataset from AVISO (https://www.aviso.altimetry.fr/) from 1990 to 2020 provides delayed-time anomaly graphs for the Sea Surface Height (SSH) Anomaly. The dataset has a resolution of 0.33° * 0.33° and is sampled every seven days. To incorporate measurements of mean sea level fluctuation, we have utilized the same SSH anomaly dataset (13.a) from a multi-satellite altimeter provided by AVISO (CNES, 2020) in this study.

Estimation of sea surface temperature

The estimation of Sea Surface Temperature (SST) between 1990-2015, is retrieved from the MODIS-Aqua (Vermote, 2015), involves using thermal infrared data and the split-window method. Sarangi & Devi (2017) used observational correlation to retrieve SST, thus following the same, the databases (CNES, 2020) are imported into a GIS framework to generate the SST scenario depicted in graph (13.b).

Results

The process of vectorizing data from raster images enabled the identification of alterations that transpired within the study area's limits of the shorelines and coastlines (Fig. 3). The positions of coastlines (Fig. 3A) and shorelines (Fig. 3B) during different years of the study period (1990-2020) have been delineated as mentioned above. Since the coastline and shorelines overlap, their differences can be observed in Fig. 3(A) and 3(B). The coastline is defined by the sea-facing edges, while the shoreline includes both the exterior sea-facing edges and the interior river bank lines. According to Figures 4 and 5, erosion and accretion rates have been varying between 1990 and 2020 along the coast of the Patharpratima block's estuarine islands. The transect-wise coastline and shoreline change rate plotted graphs illustrate the EPR in both positive and negative values.

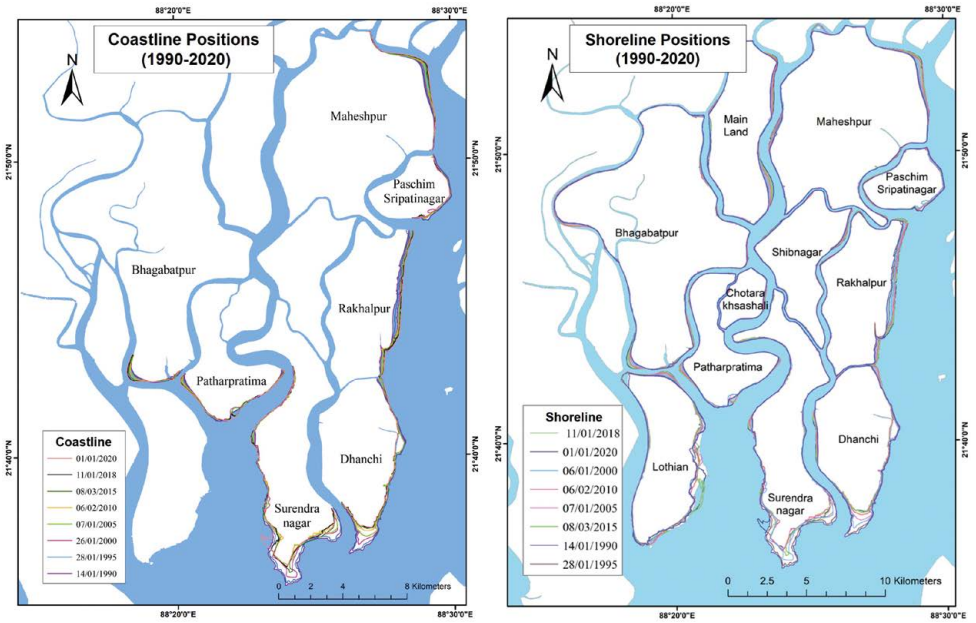

Figure 3. The estuarine islands of the Patharpratima Block: A – Coastline positions surrounding islands in the study area between 1990-2020; B – Shoreline positions around islands in the study area between 1990-2020

The estimated graph's initial right section shows substantial coastline erosion rates, reaching -56.26. The rate of sequential erosions and accretions has changed in the graph's central section. Compared to the first portion of the graph, the erosion rate in the middle section is slightly lower but more significant than the accretion rate. The mean EPR value of the graph in Figure 4 is -0.44. At the right end of the plot, the accretion rate is exceptionally high, reaching 21.19 to the EPR's overall approximation curve at this portion.

In the coastline's curve computation, the EPR plot is substantially denser than the EPR plot for the shoreline. Thus, Figure 5 shows the EPR plot of the entire shoreline of the study area, indicating a more or less fluctuating rate of erosion and accretion. There is a fluctuation between the consecutive erosion and accretion rates in the plot's initial left section. Due to the overlap in the coastal zone between shoreline and coastline, the coastline erosion rates have reached -56.26, the same rate as the shoreline erosion rates. There was a high rate of coastline accretion in the same section, up to 27.68, which is higher than the shoreline accretion rate. The middle section of the plot exhibits a relatively lower erosion rate and a higher accretion rate. This is clearly evident in the right end of the plot, where the accretion rate surpasses the erosion rate. Nevertheless, both erosion and accretion rates and intensities are lower than in the first section within this particular section of the entire EPR calculation curve.

Table 2 displays the data derived from the study area's shoreline and coastline measurement curves. In the case of coastline, where the mean value of EPR is -0.44, the highest and lowest values of EPR are -56.6 and 21.19. In the case of shoreline, the mean value of EPR is 0.36, and the highest and lowest values are -56.6 and 27.68.

The EPR values for the coastline and shoreline in the study area are depicted in Figures 4 and 5. These values are also shown

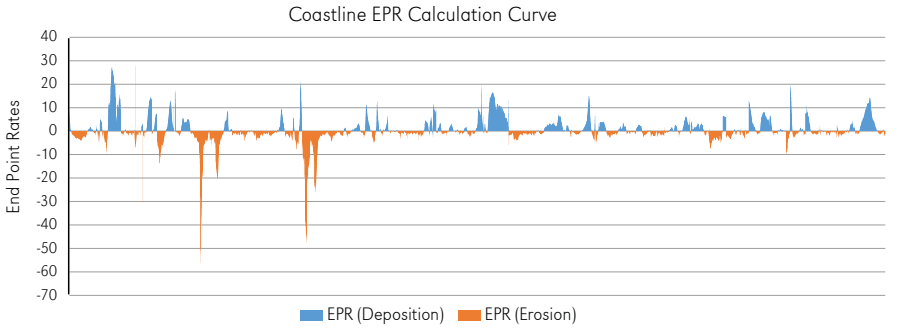

Figure 4. Endpoint rates calculation curve (blue colored curves depicting deposition, and orange-colored curves depicting erosion) of the study area's coastline

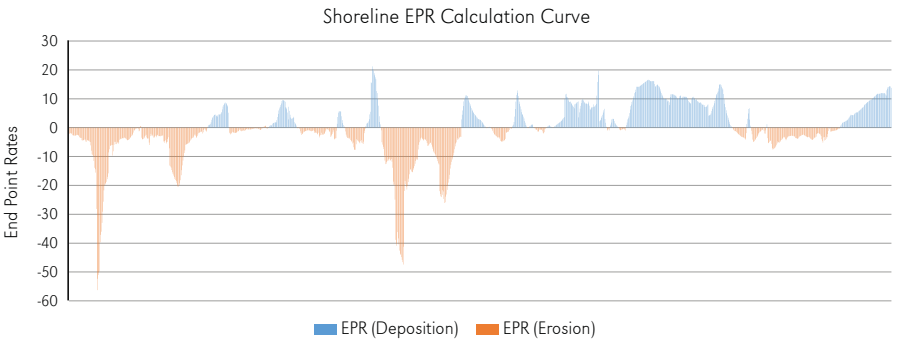

Figure 5. Endpoint rates calculation curve depicting deposition, and erosion of the study area's shoreline

on a map of the Patharpratima Block in Figure 6. Figure 6 outlines the segments and extent of erosion along the coastlines and shorelines, depicting extreme, moderate, and minimum scales of erosion. The erosion levels along Surendranagar and Dhanchi range from intense to extreme (-10.34 to -56.26), as indicated by deep green (intense) and deep blue (severe) transect lines in Figure 6(A). Moderate erosion (1.34-10.34) is evident on the shoreline across the southeast of Bhagabatpur and Patharpratima, east of Paschim Sripatnagar, and Dhanchi of Patharpratima, denoted by bright green transect lines. Marginal erosion (21.19-5.90) occurred along the east of Rakhalpur and southwest of Bhagtpur and Patharpratima. In the entirety of the study area, including the maximum portions of the shoreline, a moderate level of erosion is depicted in fluorescent green in Figure 6(B).

Table 2. Statistics of shoreline and coastline changes in EPR

EPR	Coastline	Shoreline
Maximum	-56.26	-56.26
Minimum	21.19	27.68
Mean	-0.44	0.36

Shoreline change envelope

The SCE model in this study measures the distance from the nearest shorelines to a baseline across each transect. It also records collective changes in coastal movement and considers the coastline and shoreline movement rate relative to the baseline position. Figure 7 depicts the distance between the furthest and nearest shorelines and coastlines, showing the shift from 1990 to 2020 in the research area. This illustrates the change over the study area during this time.

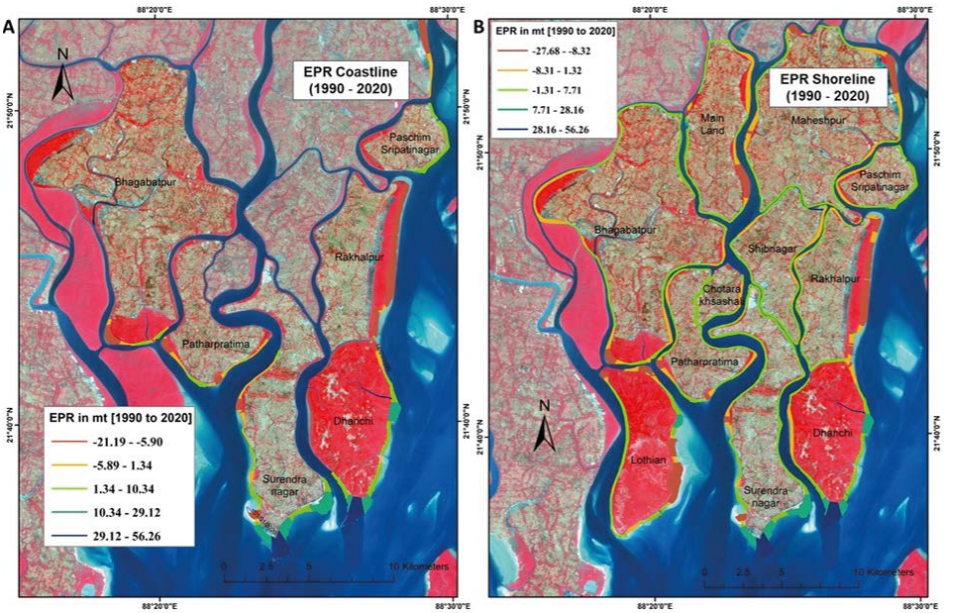

Figure 6. Transect-wise EPR of coastlines (A) and shorelines (B) around the estuarine islands of the study area during 1990-2020

The maximum shift has been observed in the southern region ranges between 872.58 and 11,685.77 meters, as depicted by the red transects. While, minimal transition (0.30-84.6 m) is seen along most coastline regions. Moderate changes in coastline (210.95-872.58 m) is observed in the southeastern and eastern edges of Surendranagar, Dhanchi, and Rakhalpur in Figure 7 (B). Lastly, minimal coastline transition is noted in the southern and southwest of Patharpratima, Bhagabatpar, and the west of Surendranagar in Figure 7 (B).

Areal extent of erosion

The study area's change in land area due to erosion or deposition between 1990 and 2020 was analyzed using spatial analysis within a GIS framework. Table 3 shows the changes in land area due to erosion and deposition along the shoreline and coastline during this period. The analysis was further divided into specific time intervals to assess erosion and deposition separately. Over the entire period, there was a total erosion of 1169.29 hectares (ha) and a total deposition of 1100.59 ha along the shoreline. Deposition was greater than erosion except for the period between 1990 and 2000 and 2010 and 2020. The coastline experienced more erosion (2252.89 ha) compared to the shoreline over the same period.

Similarly, there has been more significant deposition (1973.42 ha) along the coastline than the shoreline. However, as per table 3, the time intervals when the level of erosion exceeds the deposition level or vice versa are not common between the shoreline and coastline of the study area. Between 2005 and 2010, the shoreline encountered more deposition (248.54 ha) than erosion (245.83 ha), while across the coastline, erosion (355.14 ha) outweighed deposition (343.68 ha). Then, from 2018 to 2020, the shoreline was affected by greater erosion (71.89 ha) than deposition (63.34 ha), although, across the coastline, there has been slightly more deposition (164.86 ha) than erosion (163.30 ha).

In order to evaluate the cyclic erosion and deposition occurring across the coastlines

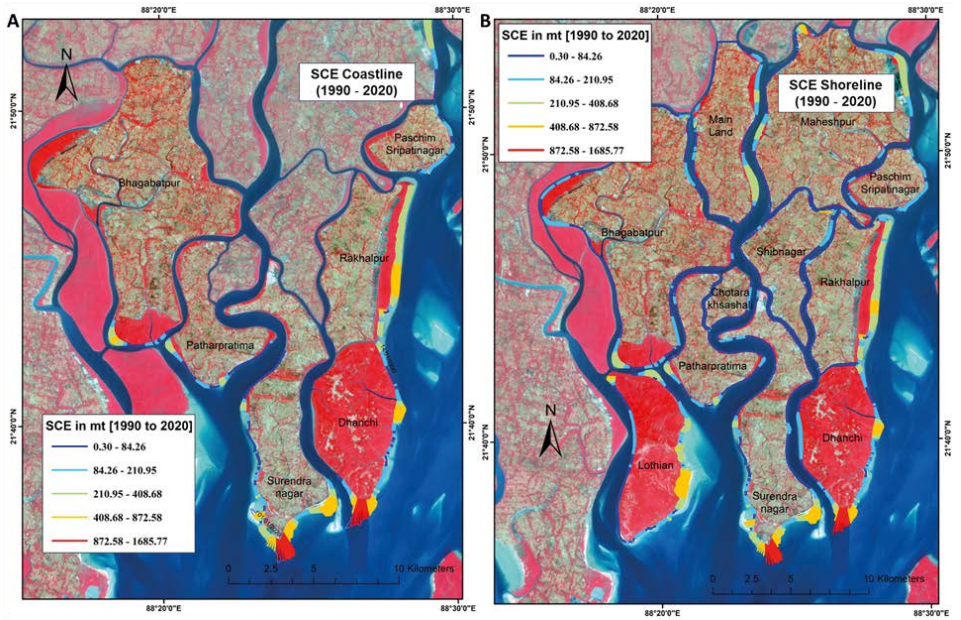

Figure 7. Transect-wise SCE around the coastlines (A) and shorelines (B) around the estuarine islands study area during 1990-2020

Table 3. The year-wise extent of erosion and deposition along the coastline and shoreline of the study area. The red colour depicts higher erosion than deposition and the green colour depicts vice-vers

Duration	Coastline				Shoreline			
	erosion [ha]	erosion [%]	deposition [ha]	deposition [%]	erosion [ha]	erosion [%]	deposition [ha]	erosion [%]
1990-1995	278.42	17.26	116.37	10.57	386.19	13.99	236.31	11.97
1995-2000	525.21	32.57	130.32	11.84	859.81	31.15	261.43	13.25
2000-2005	197.62	197.62	258.63	23.50	344.33	12.47	414.8	21.02
2005-2010	245.83	245.83	248.54	22.58	355.14	12.86	343.68	17.42
2010-2015	184.34	11.43	183.52	16.67	354.16	12.83	352.22	17.85
2015-2018	109.43	6.79	99.86	9.07	297.59	10.78	200.13	10.14
2018-2020	71.89	4.46	63.34	5.76	163.3	5.92	164.86	8.35

and shorelines, particular estuarine islands (Dhanchi, Surendranagar, Patharpratima, Rakhalpur, Paschim Sripatinagar, Bhagabatpur) of the Patharpratima block have been considered separately because they have sea-facing land interfaces known as coastlines. Then, to assess the erosion and deposition mechanisms across the shorelines, all of the islands (Lothian, Dhanchi, Surendranagar, Patharpratima, Chotarakhsashali, Rakhalpur, Shibnagar, Paschim Sripatinagar, Bhagabatpur, Maheshpur) in the study area have been taken into consideration since the shorelines cover both the coastline as well as the inward estuarine margins and river banks. The bar diagrams illustrated in Figure 8 highlight the changes in areal extent due to erosion and deposition along the coastline of the estuarine

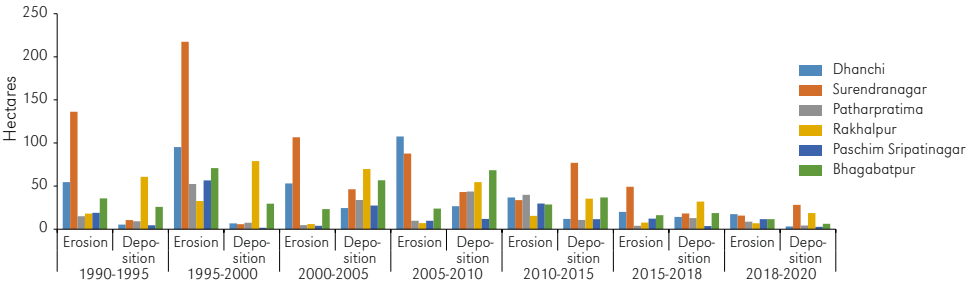

Figure 8. Comparative bar diagrams showing island-wise erosion and deposition along the coastlines of the study area

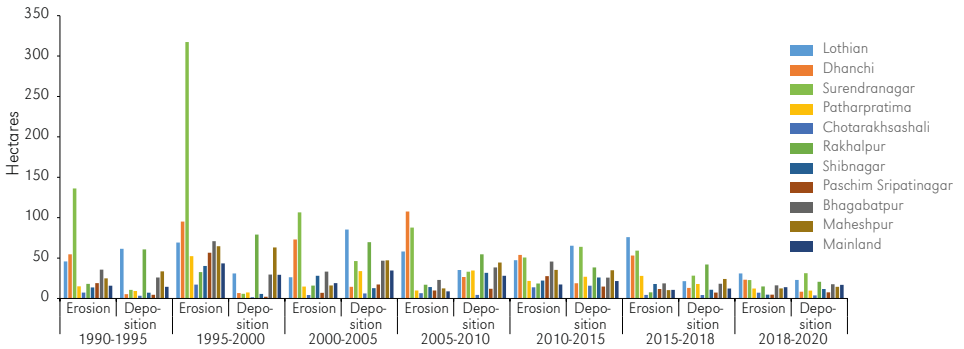

Figure 9. Comparative bar diagrams showing island-wise erosion and deposition along the shoreline of the study area

islands between 1990-2020. The most severe erosion occurred at Surendranagar (646.44 ha), followed by Dhanchi (384.85 ha) and Bhagabatpur (210.23 ha). Minimal erosion was noted at Patharpratima (122.25 ha) and Rakhalpur (93.69 ha). Maximum deposition occurred at Rakhalpur (350.46 ha), and moderate deposition was observed at Bhagbatpur (242.51 ha) and Surendranagar (229.21 ha). The least deposition was found at Dhanchi (92.46 ha) and Paschim Sripatinagar (63.69 ha).

Figure 9 illustrates the changes in the areas impacted by erosion and deposition along the shorelines of the islands from 1990 to 2020. The most significant erosion occurred in Surendranagar (780.44 ha), followed by Dhanchi (460.65 ha) and Lothian (353.74 ha). Bhagabatpur experienced a moderate level of erosion (243.38 ha), while Maheshpur (176.35 ha), Patharpratima (153.93 ha), and Shibnagar (140.97 ha) underwent less erosion. Chotarakhsashali had the least erosion (60.74 ha). During the same period, Rakhalpur experienced the highest deposition (365.46 ha), followed by Lothian (322.58 ha). It is observed that shoreline of Lothian Island is undergoing a significant and dynamic cycle of erosion and deposition, driven by intense tidal activity. Chotarakhsashali experienced minor deposition (39.51 ha), followed by Paschim Sripatinagar (65.65 ha) and Dhanchi (93.66 ha). The similar observations on broader scale regarding increasing coastal vulnerability of Pathapratima block due to tide-water encroachment has been mentioned in the study by Dhara & Paul (2023).

The gradual erosion and accretion in Patharpratima Block, as illustrated in the clear and informative Figure 10, have provided a visual understanding of the changes that occurred across the study area's shoreline and coastline between 1990 and 2020. The erosion has resulted in an aerial depletion

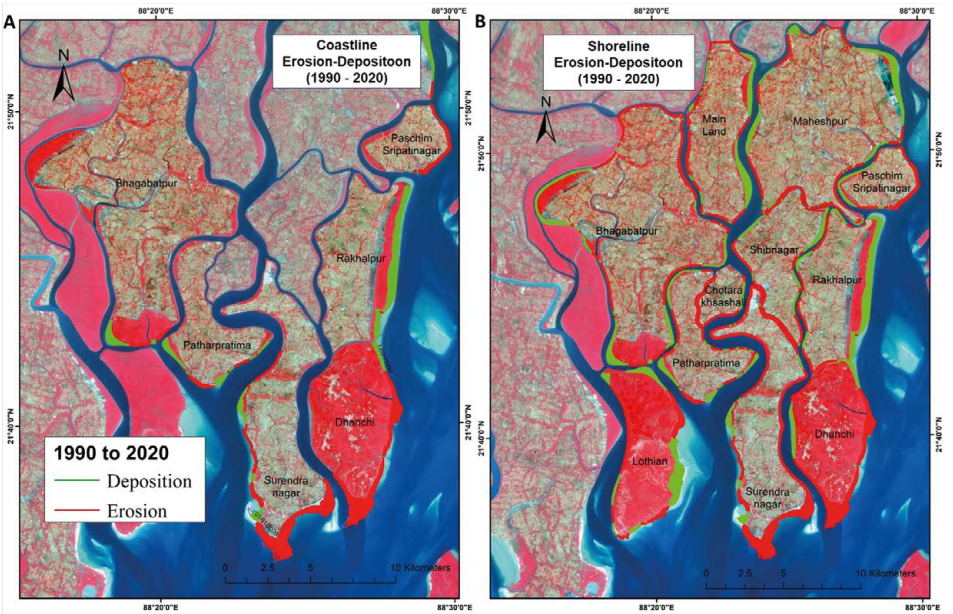

Figure 10. Scenario of erosion and deposition across the coastlines (A), and shorelines (B) of Patharpratima Block (1990-2020)

of 2760.51 ha compared to accretion, which has led to an accumulation of 1973.42 ha. The total change in the Patharpratima Block study area from 1990 to 2020 has been 789.092 ha, i.e. 7.89 km^2.

Validation of shoreline using the shore profiles

The results of the analyses have been validated by the incorporation of shore profiles and shorelines acquired through field study. The shore profile, also known as the beach profile, depicts the depth of the shoreline from the land into the water. A "shore profile" is a cross-section of a coastline drawn perpendicular to the coast's shape, including the edge of a cliff or sea wall, the backshore, the foreshore, and underwater areas close to the shore (McCracken, 2011) This method is used to analyze coastal erosion, accretion patterns, and assess beach recovery after a storm surge. In this study particular shore profiles have been obtained from the study area's coastal zones via field survey to validate the current position of the shoreline and evaluate the erosion and accretion patterns that prevailed all along the coastline/shorelines. Then, satellite imagery-derived shoreline has been incorporated to validate the current tidal datum-based shoreline location on mean sea level using GIS and remote sensing techniques.

Figure 11 displays a map showing the shoreline derived from satellite data and graphs of in-situ shore profiles based on field measurements. The shore profiles are categorized into erosion and accretion, as shown in Figure 11. The line graphs under the erosion category indicate an undercut coastal zone induced by wave erosion with uneven slopes and abrupt patterns. In contrast, the line graphs under the accretion category show a gentle and smooth pattern, indicating estuarine zones undergoing the process of accretion or deposition. The shore profiles depict erosion and accretion mechanisms at different locations along the study area's shoreline. The shore profiles obtained from Surendranagar and Paschim Sripatinagar indicate deep undercutting due to wave-induced erosion.

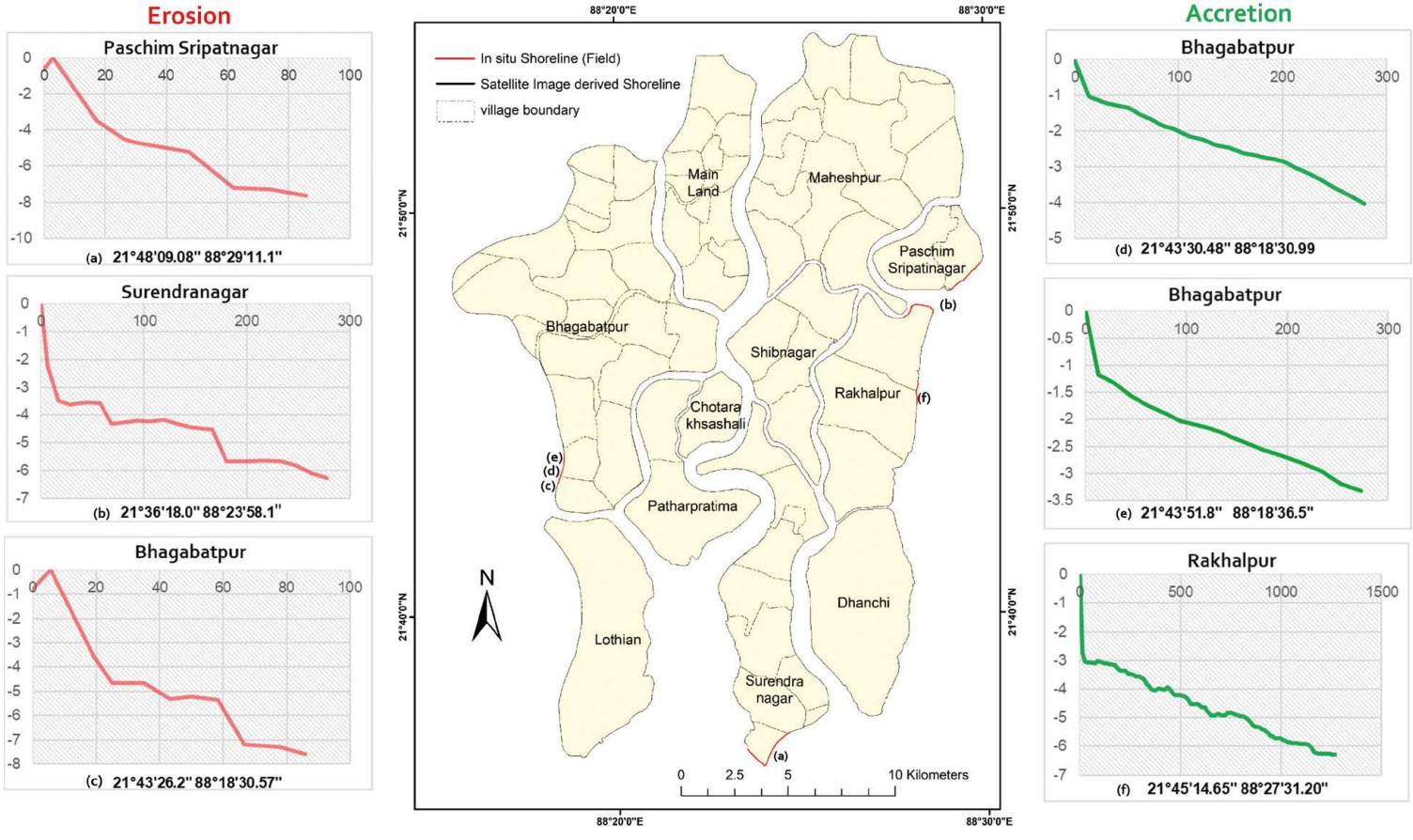

Figure 11. The line graphs represent the in-situ shore profiles measured at locations of the study area to validate the satellite-derived shoreline of the study area

Bhagabatpur's profiles show a mix of erosion and accretion mechanisms, while Rakhalpur's profile reflects a moderate slope with few undulations, indicating accretion. From the estimated shore profiles, it can be inferred that there has been a dual mechanism of erosion and accretion throughout the shoreline, as further detailed in the following section of the current study.

Predicted outcomes

The End Point Rate (EPR) model is an effective method applied in the current study to forecast changes in the study area's shoreline based on the change rate over time. In this analysis, the EPR model has been used for predicting the positions of shoreline in 2030 based on the year 2020 (Fig. 12). As mentioned previously, the total change in the Patharpratima Block from 1990 to 2020 has been 789.092 ha, i.e. 7.89 km^2.

Figure 12 depicts the predicted shoreline for 2030, which is determined by using the EPR prediction model expressed mathematically in Equations 3-6 (Awad & El-Sayed, 2021). The map in Figure 12 predicts that the shoreline and coastline will shift by 2030. It shows that erosion has caused significant retreats along the estuarine islands of Patharpratima Block, especially along the southwestern and western margins of Surendranagar and Dhanchi. The eastern and western parts of Lothian and the eastern coasts of Bhagabatpur, and Paschim Sripatnagar have also experienced negative changes due to erosion, as illustrated in Figure 12. Additionally, the northeastern and southeastern parts of the island will undergo significant shifts between the 2020 shoreline and the predicted 2030 shoreline. There have been positive changes along the northern and southern margins of Patharpratima and Bhagabatpur, resulting in a slight deposition and a more positive change in the estimated 2030 shoreline compared to 2020. Based on these findings, it can be concluded that if the current rate of change remains constant, the shoreline will correspond to the predicted 2030 shoreline shown in Figure 12.

Discussion

Compared to previous studies conducted on Patharpratima regarding coastal erosion (Chakraborty & Adhikary, 2014; Dhara & Paul, 2023; Samanta, 2018; Sreelekshmi et al., 2023), which assessed the erosion/accretion scenario of the coastline and shoreline as separate entities, this study also predicted the future scenario of the shoreline. According to the projected outcome (Fig. 12), it is anticipated that there will be a further shift in the location of the shoreline by 2030. The estimated 2030 shoreline for the estuarine islands of Patharpratima Block reveal significant retreats, with the majority of the study region's shoreline experiencing extreme erosion, as depicted in Figure 10 (B).

The study's findings indicate that between 1990 and 2020, extensive erosion took place along the southern margins of the shoreline on the islands of Surendranagar and Dhanchi. Additionally, as shown in Figure 10 (B), moderate to slight erosion has occurred along the interior margins of the shoreline to the north and northeast of Bhagabatpur, as well as to the west and south of the mainland, southeast of Maheshpur, and in Shibnagar. Several factors that have contributed to the negative change along the coastline and shoreline are considered in this study, including sea surface temperature, sea surface height, atmospheric temperature (Fig. 14 A), mangrove health, and precipitation. Sea surface temperature (SST) is the primary indicator of weather and climate in this study, and its monthly trend in the Bay of Bengal was evaluated for the period 1981 to 2015. According to Figure 13(A), the SST ranged from 25.4°C to 32°C during 1981-2015, indicating an increase in SST variability. The average SST was 28.36°C from 1981 to 1995 and 28.75°C from 1996 to 2015, representing a 0.4°C rise over the last two decades. This significant increase in SST has adverse effects on aquatic life and negatively impacts the health of the mangrove ecosystem in the Sundarbans region. The heightened SST has led to more frequent and

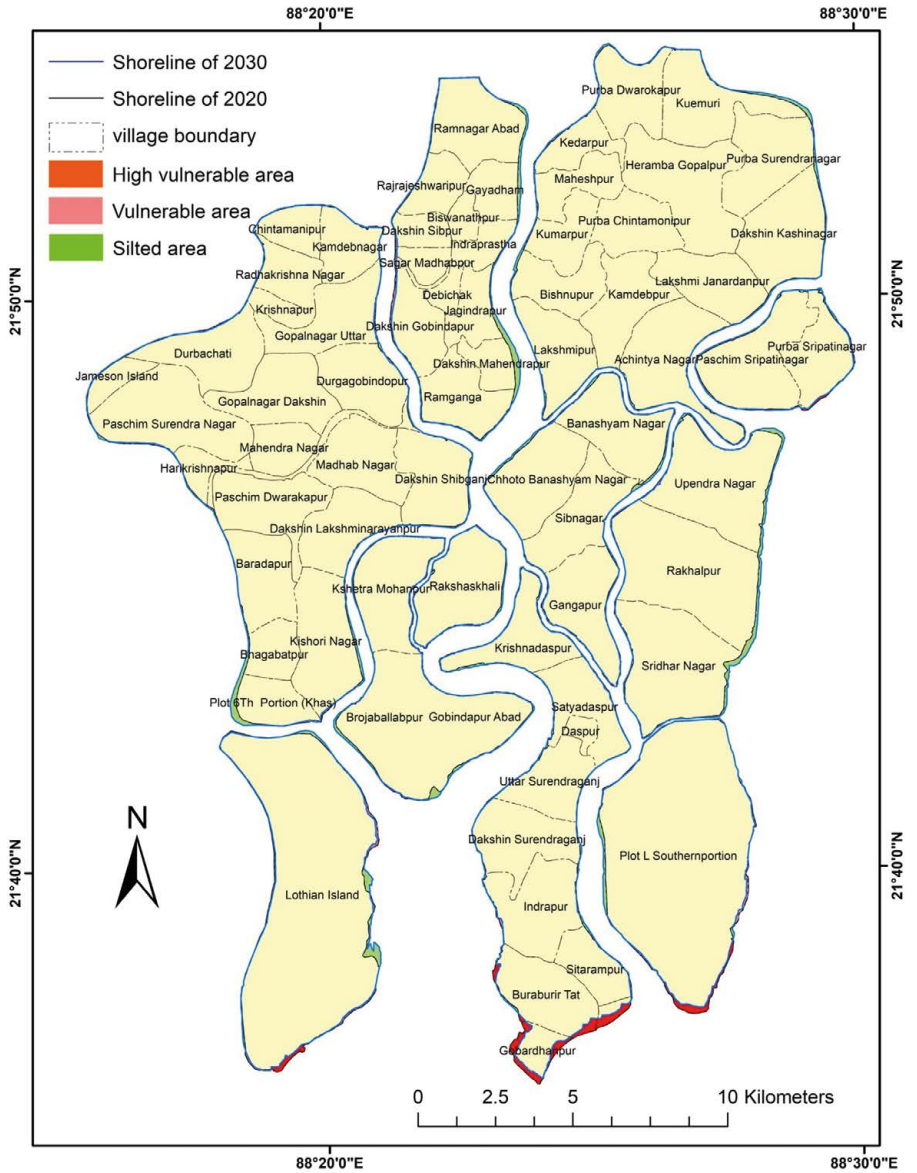

Figure 12. Shoreline of 2020 and predicted shoreline of 2030 using EPR

intense cyclones in the Sundarban Biosphere Reserve. The observed increase in annual mean SST over recent decades supports the likelihood of rising SSH. The SSH ranged from -19 mm to 28 mm from 1993 to 2014, indicating a growing sea surface height anomaly in recent decades. The annual mean SSH in the study area was 3.06 mm from 1993 to 2014 and increased to 4.94 mm from 2004 to 2014, reflecting a substantial rise of 1.88 mm in recent years. This swift rise in sea level results in more erosion than accretion along the coastline and coastline, posing a threat to the health of the study area's mangroves. This

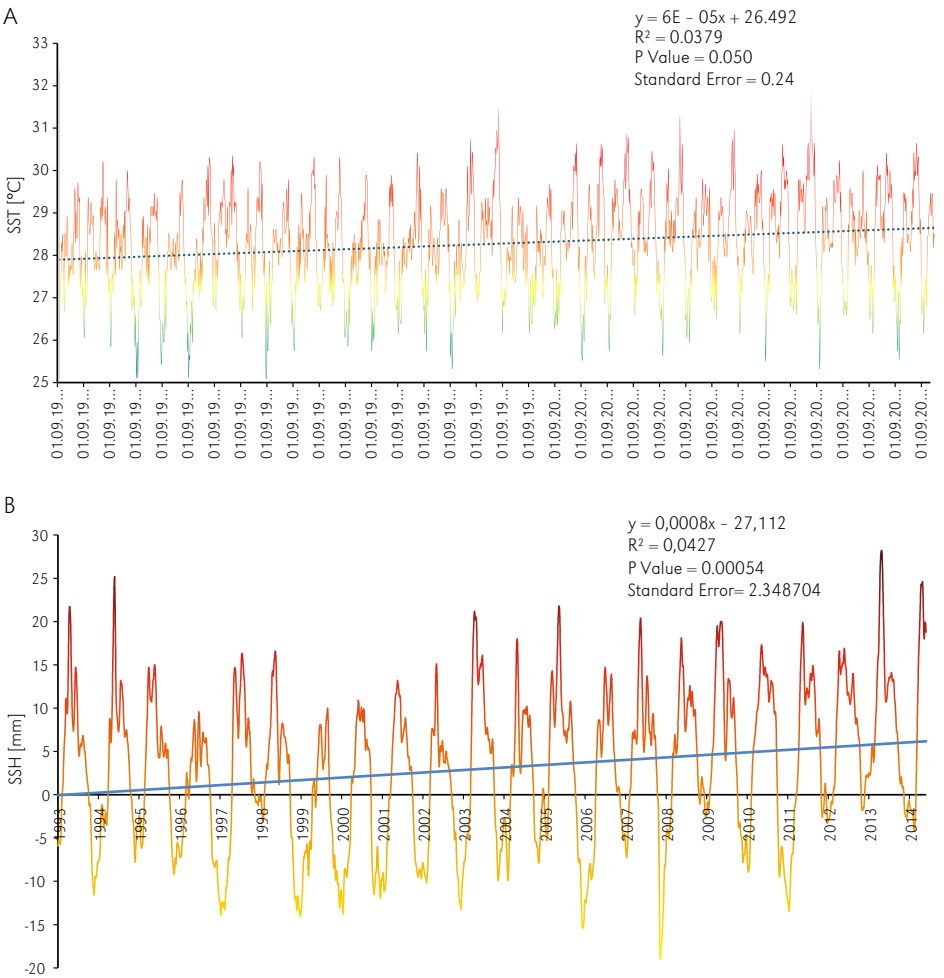

Figure 13. Sea Surface Temperature (A); Sea Surface Height (B) across study area

Source: CNES (2020); NOAA (2019).

increase in SSH is primarily responsible for the submergence of Lohachara and Supribhanga, situated west of the Patharpratima Block. In addition to sea surface temperature, the study also considered the atmospheric temperature (1990-2019) in the study area.

The average annual temperature range in 1990 was 26.2°C, and it increased to 26.9°C in 2019, indicating a significant 0.7°C rise in mean air temperature over the 29-year period. This temperature trend has the potential to intensify cyclones and lead to more powerful storm surges. From 1990 to 2020, the annual rainfall has shown significant variability, ranging from 2231.46 mm to 738.22 mm. The average rainfall between 1990 and 2010 was 1794 mm, and it decreased to 1558 mm between 2010 and 2020. This decline in annual rainfall over the past decade, as shown in Figure 14(B), is likely to increase mangrove salinity levels, affecting fertility, seedling survival, and overall mangrove diversity. These environmental changes could contribute to a decline in the mangrove

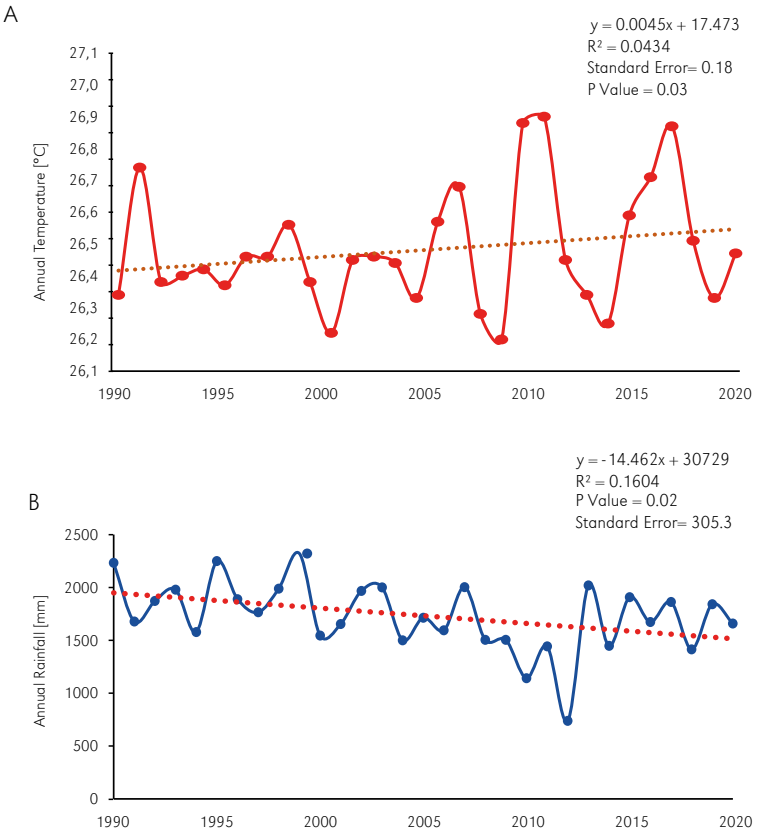

Figure 14. Annual Temperature at Patharpratima Block (A), Annual Rainfall at at Patharpratima Block (B)

Source: NASA Power.

region (Sandilyan, 2015). Thus, salinization of the low-lying region of Patharpratima due to tidal intrusion is causing river bank erosion, a phenomenon also observed in the study by Chakraborty and Adhikary (2014).

Apart from these environmental factors, the total population of Patharparatima (1981-2021) has been considered a factor for this study. Figure 15 illustrates a line graph showing an upward population curve, showing that the human population in the study area increased from 197,686 in 1981 to 331,823 in 2011. This trend highlights a crucial between the growth and density of the human population and the loss of mangrove coverage in the Indian Sundarbans. The exponential increase in the number of people living near mangrove areas, along with the growing demand for resources, has resulted in significant deforestation and degradation of these ecosystems. The local communities often exploit these ecosystems for agriculture, aquaculture, and other means of livelihood (Uddin, 2018). The degradation of mangroves can lead to the significant release of carbon dioxide (CO2) that is stored within them. Since mangroves are among the most carbon-rich forests in the tropics (UN-DESA, 2020), their destruction or degradation can contribute to climate change by allowing this greenhouse gas to enter the atmosphere. (Uddin et al., 2023).

Conversely, the loss of these ecosystems intensified climate change impact, increasing the severity and frequency of storm surges

and cyclones, resulting in the loss of mangrove buffer zones and displacement of livelihood. Climate change has altered the monsoonal precipitation patterns, driven SLR, and significantly increased SST (Fig. 13A), posing a serious threat to the region under study (Datta et al., 2024).

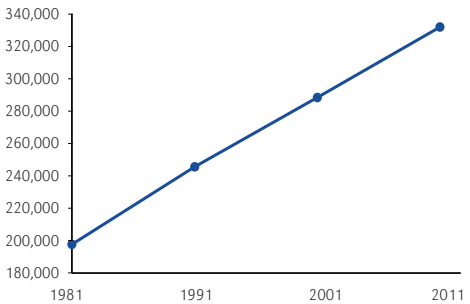

Figure 15. The population size of the study area between 1981-2021

Source: WorldPop, 2018.

Considering the significant role that mangroves play in coastal erosion, it is essential to include the health of vegetation in this study. The health of mangrove vegetation from 1990 to 2020 can provide insights into the effects of various factors on the existing mangrove habitats in the area under investigation. Figure 16 shows mangrove health in the study area from 1990 to 2020 using NDVI values in a line graph. NDVI, derived from the R(Red) and NIR band on the EM (Electromagnetic) spectrum, known as NDVI, can depict biomass or greenish level. NDVI values range from -1 to +1, but the values that indicate the mangrove health range between +0.1 and +0.7. As per Figure 13, the fluctuating nature of mangrove health can be observed between 1990 and 1995, mainly because of the fluctuating level of factors mentioned above (rainfall, temperature, SST, SSH). The mangrove health ranges from lesser to moderately vulnerable. The line in Figure 16 represents the NDVI value, which is curved further downward by 2000, indicating deterioration in mangrove health; again, the line curved upward between 2005 and 2010, indicating enhanced mangrove health. After 2010, the line has curved further downward, indicating further deterioration in mangrove health, posing a higher vulnerability.

Furthermore, despite the decrease in the area of Patharpratima, it is crucial to note that the area is protected by 249 km of embankments along rivers. These embankments are of critical importance for safeguarding lives and protecting crops from daily tidal effects, monsoonal flooding, and storm surges (Dhara & Paul, 2016). However, if this situation of coastal erosion persists, it will undoubtedly lead to significant risks in the near future

As mentioned above, mangroves are natural barriers against extreme weather and coastal erosion; however, their decline, as

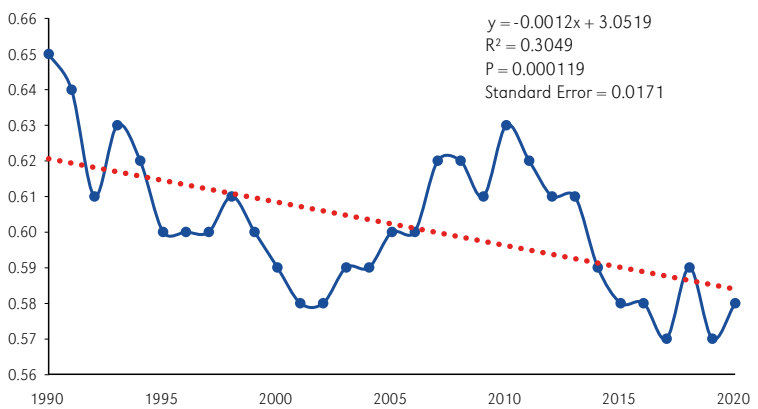

Figure 16. Mangrove vegetation health in Patharpratima Block

evidenced in the Figure 16, has worsened erosion, resulting in loss of livelihoods. Hence, the Sustainable Development Goal (SDG) 11, aiming towards an inclusive, protected, resilient, and sustainable community, must be achieved with a focus on conserving the mangroves of the Sundarbans (Livelihoods Funds, 2020). Restoring and protecting these ecosystems is essential for improving resilience against coastal erosion and the impacts of climate change. Therefore, to control erosion along the coastline, and shoreline it is imperative to enhance the health of coastal mangroves and expand vegetative cover on the islands of the Patharpratima Block. This can be achieved through ground plantation, including the planting of mangroves, Caesarians, and bamboo. The robust growth of trees and shrubs on the river banks not only regulates the flow rate, but also the velocity distribution within the river's profile. Woody vegetation along all coastlines in natural river systems does not hinder floodwater drainage, as there is ample space in the river corridor to manage heavy runoff effectively. These efforts are key to achieving SDG 13 (Climate Action) and SDG 14 (Life Below Water), as they can enhance climate change resilience and strengthen economic support for local communities (UNRIC, 2022).

Conclusion

The research was conducted using advanced computational techniques on multi-resolution satellite data to extract detailed information about the shoreline and coastline of the islands located in the Patharpratima Block. This information was integrated into the geospatial interface of the statistical model of DSAS. Thereafter, using this statistical modelling framework in a GIS environment, a multi-directional analysis was conducted on the study to acquire a comprehensive scenario. A field-based shore profile analysis was also conducted to supplement the results further. The results obtained from the study depicted the complex and dynamic behaviour of the coastline and shoreline. It was observed that significant degradation took place between 1990 and 2020 compared to the rest of the coastline. The study also revealed that subregions like Dhanchi and Surendranagar had experienced very high erosion along their respective shorelines and coastlines (-10.34 to -56.26) compared to others. However, based on overall analysis, it can be stated that the erosion rates across the estuarine islands in the Patharpratima Block are highly alarming, which highlights the effect of rising sea levels and the urgency for adopting measures to prevent any further degradation of the coastline and shoreline to protect the lives of the inhabitants in the area. The study's results underscore the need for a proactive approach to mitigate the effects of erosion, especially in areas vulnerable to high erosion rates. This is particularly concerning as these landmasses are inhabited, and the trend of erosion continues to pose a grave concern for the residents of Patharpratima Block, emphasizing the importance of prevention over reaction.

Editors' note:
Unless otherwise stated, the sources of tables and figures are the authors', on the basis of their own research.

References

Acharyya, R., Mukhopadhyay, A., & Habel, M. (2023). Coupling of SWAT and DSAS Models for Assessment of Retrospective and Prospective Transformations of River Deltaic Estuaries. *Remote Sensing*, *15*(4), 958. https://doi.org/10.3390/rs15040958

Adarsa, J., Shamina, S., & Arkoprovo, B. (2012). Morphological Change Study of Ghoramara Island, Eastern India Using Multi Temporal Satellite Data. *Research Journal of Recent Sciences*, *1*(10), 72-81.

Alongi, D. M. (1998). *Coastal Ecosystems Processes*. Boca Raton, FL, USA: CRC Press.

Awad, M., & El-Sayed, H. M. (2021). The analysis of shoreline change dynamics and future predictions using automated spatial techniques: Case of El-Omayed on the Mediterranean coast of Egypt. *Ocean & Coastal Management*, *205*. https://doi.org/https://doi.org/10.1016/j.ocecoaman.2021.105568

Basu, J. (2019). Bulbul 'more dangerous than Aila': Affected people. Down To Earth. https://www.downtoearth.org.in/natural-disasters/bulbul-more-dangerous-than-aila-affected-people-67805

Bhattacharya, B. D., Bhattacharya, A. K., Rakshit, D., & Sarkar, S. K. (2014). *Impact of the tropical cyclonic storm 'Aila'on the water quality characteristics and mesozooplankton community structure of Sundarban mangrove wetland, India*. *Indian Journal of Geo-Marine Sciences*, *43*(2), 216-223.

Bheeroo, R. A., Chandrasekar, N., Kaliraj, S., & Magesh, N. S. (2016). Shoreline change rate and erosion risk assessment along the Trou Aux Biches–Mont Choisy beach on the northwest coast of Mauritius using GIS-DSAS technique. *Environmental Earth Sciences*, *75*(5). https://doi.org/10.1007/s12665-016-5311-4

Brown, S., & Nicholls, R. J. (2015). Subsidence and human influences in mega deltas: The case of the Ganges–Brahmaputra–Meghna. *Science of The Total Environment*, *527-528*, 362-374. https://doi.org/https://doi.org/10.1016/j.scitotenv.2015.04.124

Central Water Commission. (2016). *Status Report on Coastal Protection & Development in India*. 120. http://cwc.gov.in

Chakraborty, S., & Adhikary, M. (2014). Vulnerability and risk assessment of environmental hazards – A case study of Patharpratima Block,(Sundarban Delta Region) South 24 Parganas, West Bengal, India. *IOSR Journal of Environmental Science, Toxicology and Food Technology*, *8*, 67-87.

CNES. (2020). AVISO. IEEE Transactions on Geoscience and Remote Sensing. https://www.aviso.altimetry.fr/en/home.html

Columbia University. (2020). *Coastal Processes*. Columbia University in the City of New York. http://www.columbia.edu/~vjd1/coastal_basic.htm

Committee on Climate Change. (2010). Managing the environment in a changing climate. https://assets.publishing.service.gov.uk/media/5a75c59040f0b6488c78ed6d/geho0111btjy-e-e.pdf

Das, S., Das, A., Kar, N. S., & Bandyopadhyay, S. (2020). Cyclone Amphan and its impact on the Lower Deltaic West Bengal: a preliminary assessment using remote sensing sources. *Current Science*, *119*(8), 1246-1249. https://www.jstor.org/stable/27139008

Datta, P., Behera, B., & Rahut, D. B. (2024). Climate change and water-related threats in the Indian Sundarbans: food security and management implications. *International Journal of Water Resources Development*, *40*(3), 323-344. https://doi.org/10.1080/07900627.2023.2224459

Dhara, S. (2019). Physical environmental setting of the Hugli – Saptamukhi estuarine deltaic complex in South West Sundarban, West Bengal. *Journal of Emerging Technologies and Innovative Research, 6*(2), 48-57. https://www.jetir.org/papers/JETIR1902A72.pdf

Dhara, S., & Paul, A. K. (2016). Status of agriculture: A case study at Patharpratima Block of South 24 Parganas District. *International Journal of Innovative Science, Engineering & Technology*, *3*(2), 239-246. https://ijiset.com/vol3/v3s2/IJISET_V3_I2_34.pdf

Dhara, S., & Paul, A. K. (2023). Assessment of Hazards and Flood Risks in the Southwestern Sundarbans. In A. K. Paul & A. Paul (Eds.), *Crisis on the Coast and Hinterland: Assessing India's East Coast with Geomorphological, Environmental and Remote Sensing and GIS Approaches* (pp. 229-239). Springer Nature Switzerland. https://doi.org/10.1007/978-3-031-42231-7_17

European Space Agency. (2020). *Sea Surface Height*. https://sentiwiki.copernicus.eu/web/synergy-applications#:~:text=SSH%20is%20the%20height%20of,with%20respect%20to%20the%20geoid.

Farquharson, L. M., Mann, D. H., Swanson, D. K., Jones, B. M., Buzard, R. M., & Jordan, J. W. (2018). Temporal and spatial variability in coastline response to declining sea-ice in northwest Alaska. *Marine Geology*, *404*, 71-83. https://doi.org/https://doi.org/10.1016/j.margeo.2018.07.007

FitzGerald, D. M., Fenster, M. S., Argow, B. A., & Buynevich, I. V. (2008). Coastal impacts due to sea-level rise. *Annual Review of Earth and Planetary Sciences*, *36*, 601-647. https://doi.org/10.1146/annurev.earth.35.031306.140139

Geological Survey Ireland. (2020). *Coastal Erosion*. Geological Survey Ireland. https://www.gsi.ie/en-ie/geoscience-topics/natural-hazards/Pages/Coastal-Erosion.aspx#:~:text=Abrasion is when rocks and,carried away by the sea.&text=Attrition is when material such,each other wearing them down.

Ghosh, S., Hazra, S., Nandy, S., Mondal, P. P., Watham, T., & Kushwaha, S. P. S. (2018). Trends of sea level in the Bay of Bengal using altimetry and other complementary techniques. *Journal of Spatial Science*, *63*(1), 49-62. https://doi.org/10.1080/14498596.2017.1348309

Ghosh, T., Bhandari, G., & Hazra, S. (2001). Assessment of Landuse/ Landcover Dynamics and Shoreline Changes of Sagar Island Through Remote Sensing. *22nd Asian Conference on Remote Sensing*, *January*, 43.

Ghosh, T., Hajra, R., & Mukhopadhyay, A. (2014). Island erosion and afflicted population: Crisis and policies to handle climate change. In *International Perspectives on Climate Change: Latin America and Beyond* (pp. 217-225).

Halder, B., & Bandyopadhyay, J. (2022). Monitoring the tropical cyclone 'Yass' and 'Amphan'affected flood inundation using Sentinel-1/2 data and Google Earth Engine. *Modeling Earth Systems and Environment*, *8*(3), 4317-332. https://doi.org/10.1007/s40808-022-01359-w

Hasanuzzaman, Md., Islam, A., Bera, B., & Shit, P. K. (2023). Quantifying the riverbank erosion and accretion rate using DSAS model study from the lower Ganga River, India. *Natural Hazards Research*. https://doi.org/https://doi.org/10.1016/j.nhres.2023.12.015

Hazra, S., Mukhopadhyay, A., Mukherjee, S., Akhand, A., Chanda, A., Mitra, D., & Ghosh, T. (2016). Disappearance of the New Moore Island from the southernmost coastal fringe of the Sundarban Delta – A case study. *Journal of the Indian Society of Remote Sensing*, *44*(3), 479-484. https://doi.org/10.1007/s12524-015-0524-7

Hazra, S., & Samanta, K. (2016). *Temporal Change Detection (2001-2008): Study of Sundarban*.

Himmelstoss, E. A., Henderson, R. E., Kratzmann, M. G., & Farris, A. S. (2018). Digital Shoreline Analysis System (DSAS) Version 5.0 User Guide. In *U.S. Geological Survey*. https://doi.org/https://doi.org/10.3133/ofr20181179.

Huang, C., Wylie, B., Yang, L., & Homer, C. (2002). Derivation of a tasselled cap transformation based on Landsat 7 at-satellite reflectance. *International Journal of Remote Sensing*, *23*(8), 1741-1748. https://doi.org/http://dx.doi.org/10.1080/01431160110106113

Inman, D. L., Jenkins, S. A., McLachlan, A., Orme, A. R., Leatherman, S. P., Whitman, D., Zhang, K., ... & Bird, E. (2005). A BT. In M. L. Schwartz (Ed.), *Encyclopedia of Coastal Science*. *Encyclopedia of Earth Science Series* (pp. 1-116). Springer Netherlands. https://doi.org/10.1007/1-4020-3880-1_1

Kar, N. S., & Basu, A. (2023). A cyclone preparedness plan for the coastal blocks of the Indian Sundarban. *Journal of Coastal Conservation*, *27*(5), 49. https://doi.org/10.1007/s11852-023-00978-4

Kundu, K., & Mandal, J. K. (2024). Shoreline change detection and future prediction of Sundarban Delta using remote sensing data and digital shoreline analysis system. *Journal of the Indian Society of Remote Sensing*, *52*(3), 485-503. https://doi.org/10.1007/s12524-024-01833-1

Kundu, S., Mondal, A., Khare, D., Mishra, P. K., & Shukla, R. (2014). Shifting shoreline of Sagar Island Delta, India. *Journal of Maps*, *10*(4), 612-619. https://doi.org/10.1080/17445647.2014.922131

Li, Y., Chen, B. M., Wang, Z. G., & Peng, S. L. (2011). Effects of temperature change on water discharge, and sediment and nutrient loading in the lower Pearl River basin based on SWAT modelling. *Hydrological Sciences Journal*, *56*(1), 68-83. https://doi.org/10.1080/02626667.2010.538396

Livelihoods Funds. (2020). *INDIA (Sundarbans): 16 million mangrove trees to protect local communities*. https://livelihoods.eu/portfolio/news-india/

Maiti, S., & Bhattacharya, A. K. (2009). Shoreline change analysis and its application to prediction: A remote sensing and statistics based approach. *Marine Geology*, *257*(1-4), 11-23. https://doi.org/10.1016/j.margeo.2008.10.006

Mandal, P., Maiti, A., Paul, S., Bhattacharya, S., & Paul, S. (2022). Mapping the multi-hazards risk index for coastal block of Sundarban, India using AHP and machine learning algorithms. *Tropical Cyclone Research and Review*, *11*(4), 225-243. https://doi.org/https://doi.org/10.1016/j.tcrr.2023.03.001

Mandal, S. (2021). Geospatial framework for erosion zone identification on geospatial cloud computing. *International Journal of Innovative Science, Engineering & Technology*, *8*(6), 337-345. https://ijiset.com/vol8/v8s6/IJISET_V8_I06_36.pdf

Mangor, K., Drønen, N. K., Kaergaard, K. H., & Kristensen, S. E. (2017). *Shoreline Management Guidelines*.

Marchand, M. (2010). *Concepts and science for coastal erosion management*: *Concise report for policy makers*.

Masselink, G., & Russell, P. (2013). Impacts of climate change on coastal erosion. *MCCIP Science Review*, *1*(June), 71-86. https://doi.org/10.14465/2013.arc09.071-086

McCracken, M. (2011). *beach profile*. TeachMeFinance.Com. http://www.teachmefinance.com/Scientific_Terms/beach profile.html

McSweeny, R. (2020). *Explainer: Nine 'tipping points' that could be triggered by climate change*. Carbon Brief. https://www.carbonbrief.org/explainer-nine-tipping-points-that-could-be-triggered-by-climate-change

Mohan, R. K. (2005). Capping of contaminated coastal areas. In M. L., Schwartz (Eds.), *Encyclopedia of Coastal Science. Encyclopedia of Earth Science Series* (pp. 216-217), *14*. Dordrecht: Springer. https://doi.org/10.1007/1-4020-3880-1_59

Mohr, M. C. (2001). *Site Characterization* (Issue Part V)

Mukherjee, N., & Siddique, G. (2018). Climate change and vulnerability assessment in Mousuni Island: South 24 Parganas District. *Spatial Information Research*, *26*(2), 163-174. https://doi.org/10.1007/s41324-018-0168-0

Mukhopadhyay, A., Mukherjee, S., Mukherjee, S., Ghosh, S., Hazra, S., & Mitra, D. (2012). Automatic shoreline detection and future prediction: A case study on Puri coast, Bay of Bengal, India. *European Journal of Remote Sensing*, *45*(1), 201-213. https://doi.org/10.5721/EuJRS20124519

Nandi, S., Ghosh, M., Kundu, A., Dutta, D., & Baksi, M. (2016). Shoreline shifting and its prediction using remote sensing and GIS techniques: a case study of Sagar Island, West Bengal (India). *Journal of Coastal Conservation*, *20*(1), 61-80. https://doi.org/10.1007/s11852-015-0418-4

NASA Power. https://power.larc.nasa.gov/data-access-viewer/

Nassar, K., Mahmod, W. E., Fath, H., Masria, A., Nadaoka, K., & Negm, A. (2019). Shoreline change detection using DSAS technique: Case of North Sinai coast, Egypt. *Marine Georesources and Geotechnology*, *37*(1), 81-95. https://doi.org/10.1080/1064119X.2018.1448912

Nath, A., Koley, B., Saraswati, S., Choudhury, T., Um, J. S., & Ray, B. C. (2022). Geospatial analysis of short term shoreline change behavior between Subarnarekha and Rasulpur estuary, east coast of India using intelligent techniques (DSAS). *GeoJournal*. https://doi.org/10.1007/s10708-022-10683-8

National Geographic Society. (2020). Erosion. In *National Geographic* (pp. 1-13).

National Ocean Service. (2020). *Longshore Currents*. National Oceanic and Atmospheric Administration. https://oceanservice.noaa.gov/education/tutorial_currents/03coastal2.html#:~:text=Rather%2C they arrive at a,called a "longshore current."

Nehra, V. (2016). A Study of Coastal Erosion & Its Causes, Effects and Control Strategies. *International Journal of Research and Scientific Innovation*, *3*(6), 133-135.

NOAA. (2019). *Sea level anomaly and geostrophic currents, multi-mission, global, optimal interpolation, gridded*. NOAA Laboratory for Satellite Altimetry. https://coastwatch.noaa.gov/cwn/products/sea-level-anomaly-and-geostrophic-currents-multi-mission-global-optimal-interpolation.html

Oliver-Smith, A. (2009). *Sea Level Rise and the Vulnerability of Coastal Peoples*. InterSecTions (No. 7). United Nations University.

Oppenheimer, M., Glavovic, B., Hinkel, J., van de Wal, R., Magnan, A. K., Abd-Elgawad, A., ... & Sebesvari, Z. (2019). Sea Level Rise and Implications for Low Lying Islands, Coasts and Communities In *IPCC Special Report on the Ocean and Cryosphere in a Changing Climate* [H.-O. Pörtner, D.C. Roberts, V. Masson-Delmotte, P. Zhai, M. Tignor, E. Poloczanska, K. Mintenbeck, A. Alegría, M. Nicolai, A. Okem, J. Petzold, B. Rama, N.M. Weyer (Eds.)]. Cambridge University Press, Cambridge, UK and New York, NY, USA, pp. 321-445. https://doi.org/10.1017/9781009157964.006

Oyedotun, T. D. T. (2014). Shoreline Geometry: DSAS as a Tool for Historical Trend Analysis. *Geomorphological Techniques (Online Edition)*, *2*, 1-12.

Paice, R., & Chambers, J. (2016). *Climate change impacts on coastal ecosystems*. Coast Adapt, Impact Sheet 8. https://coastadapt.com.au/sites/default/files/factsheets/T312_9_Coastal_Ecosystems.pdf

Paul, S., & Chowdhury, S. (2021). Investigation of the character and impact of tropical cyclone Yaas: a study over coastal districts of West Bengal, India. *Safety in Extreme Environments*, *3*, 219-223. https://doi.org/10.1007/s42797-021-00044-y

Paul, S., Mishra, M., Pati, S., Acharyya, T., Santos, C. A. G., Silva, R. M. da, Guria, R., & Laksono, F. X. A. T. (2024). Evaluation of overwash vulnerability and shoreline dynamics in cyclone-prone Sagar Island, Sundarbans (India). *Science of The Total Environment*, *907*. https://doi.org/10.1016/j.scitotenv.2023.167933

Pramanick, N., Islam, E., Banerjee, S., Mukherjee, R., Maity, A., Acharyya, R., Chanda, A., Pal, I., & Mukhopadhyay, A. (2022). Threats from sea level rise and erosion: A case study of an estuarine inhabited Island Ghoramara, Hooghly Estuary. In *Urban Ecology and Global Climate Change* (pp. 321-345). https://doi.org/10.1002/9781119807216.ch16

Prasad, D. H., & Kumar, N. D. (2014). Coastal Erosion Studies – A Review. *International Journal of Geosciences*, *5,* 341-345. https://doi.org/10.4236/ijg.2014.53033

Remote Sensing Systems. (2020). *Sea Surface Temperature*. http://www.remss.com/measurements/sea-surface-temperature/#:~:text=Sea surface temperature is a,buoys%2C and ships of opportunity.&text=For instance%2C most buoys have,intervals along a tether line

Roberts, J. (2019). *What's The Difference Between Coastline And Shoreline?*. https://medium.com/@jenniferroberts050_60595/whats-the-difference-between-coastline-and-shoreline-982fcebf3ada

Rukhsana, & Hasnine, M. (2024). Delineation of multi hazards vulnerable zone using the Geospatial approach: A micro-region level study in Indian Coastal Sundarban. *Regional Studies in Marine Science*, *71*. https://doi.org/https://doi.org/10.1016/j.rsma.2024.103402

Saadi, M. L. K. (2010). *Hurricane Sidr claims beautiful mangroves*. https://islamonline.net

Samanta, B. (2018). Coastal erosion in Gabardhanpur and surrounding area, Patharpratima, South 24 Parganas, West Bengal, India. *Journal of Geography, Environment and Earth Science International*, *15*(3), 1-10. https://doi.org/10.9734/JGEESI/2018/41617

Sandilyan, S. (2015). *Climate change threatens Indian mangroves*. India Water Portal. https://www.indiawaterportal.org/climate-change/climate/climate-change-threatens-indian-mangroves

Sarangi, R. K., & Devi, K. N. (2017). Space-based observation of chlorophyll, sea surface temperature, nitrate, and sea surface height anomaly over the Bay of Bengal and Arabian Sea. *Advances in Space Research*, *59*(1), 33-44. https://doi.org/10.1016/j.asr.2016.08.038

Scott, B. D. (2005). Coastal changes, rapid. In I. Schwartz (Ed.), *Encyclopedia of Coastal Science* (pp. 233-255). Dordrecht: Springer Netherlands. https://doi.org/10.1007/1-4020-3880-1_76

Smithsonian. (2020). *Currents, Waves, and Tides*. Smithsonian – National Museum of Natural History. https://ocean.si.edu/planet-ocean/tides-currents/currents-waves-and-tides

Sondi, I., Lojen, S., Juračić, M., & Prohić, E. (2008). Mechanisms of land–sea interactions – the distribution of metals and sedimentary organic matter in sediments of a river-dominated Mediterranean karstic estuary. *Estuarine, Coastal and Shelf Science*, *80*(1), 12-20. https://doi.org/10.1016/j.ecss.2008.07.001

Sreelekshmi, S., Nandan, S. B., & Harikrishnan, M. (2023). Changes in Shoreline and Its Impact on Mangrove Structure in Selected Islands of Sundarbans, Northeast Coast of India. *Thalassas: An International Journal of Marine Sciences*, *39*(1), 343-356. https://doi.org/10.1007/s41208-022-00491-9

Thakur, S., Mondal, I., Bar, S., Nandi, S., Ghosh, P. B., Das, P., & De, T. K. (2021). Shoreline changes and its impact on the mangrove ecosystems of some islands of Indian Sundarbans, North-East coast of India. *Journal of Cleaner Production*, *284*. https://doi.org/https://doi.org/10.1016/j.jclepro.2020.124764

Uddin, M. M., Abdul Aziz, A., & Lovelock, C. E. (2023). Importance of mangrove plantations for climate change mitigation in Bangladesh. *Global Change Biology*, *29*(12), 3331-3346. https://doi.org/10.1111/gcb.16674

Uddin, S. (2018). *Life in the Sundarbans Mangrove Forest*: *Cultural Beliefs, Religious Practices, and Environmental Degradation*. https://uddin.digital.conncoll.edu/sundarbans/

UN-DESA. (2020). *The Community of Ocean Action for Mangroves – Towards the Implementation of SDG14*. https://www.cbd.int/cooperation/pavilion/cancun-

UNRIC. (2022). *Mangroves for sustainable development*. United Nations. https://unric.org/en/mangroves-for-sustainable-development/

Vermote, E. (2015). *MOD09A1 MODIS Surface Reflectance 8-Day L3 Global 500m SIN Grid V006*. ASA EOSDIS Land Processes DAAC. https://modis.gsfc.nasa.gov/data/dataprod/mod09.php

WorldPop. (2018). The Spatial distribution of population in 2000 India. In *WorldPop Open Spatial Demographic Data and Research*. https://doi.org/10.5258/SOTON/WP00645

Yincan et al, Y. (2017). Coastal Erosion. *Marine Geo-Hazards in China*, 269-296. https://doi.org/10.1016/b978-0-12-812726-1.00007-3

Article first received • 7 June 2024
Article accepted • 15 May 2025